Methods for Phase Diagram Determination of Argon via Molecular Dynamics

Álvaro Bermejillo Seco (5579244), Daniel Bedialauneta Rodríguez (5567025), and Marc Serra Peralta (5623510)

ABSTRACT

In this report, we perform molecular dynamics simulations to study various phase transition points of Argon. A symplectic integrator, namely the velocity-Verlet algorithm, is used to integrate Newton's equations of motion of N classical particles. The atoms are located inside a box with periodic boundary conditions, and are subject to the Lennard-Jones pairwise interaction. Equilibrium at the desired temperature is reached through velocity rescalings and then evolved for a certain amount time to compute various observables using time averages. The observables include the pair correlation function, pressure, diffusion constant, mean-squared displacement, and specific heat. From the pressure-density isotherms, we determine the critical point of argon using $N = 864$ particles, resulting in a critical temperature range $T_c \in [149, 176]$ K and density $\rho_c \in [504, 840]$ kg/m^3 which agrees with $T_c = 151$ K reported in literature. Moreover, the abrupt change of the diffusion constant and other observables allows us to determine the T, P points for solid-liquid and solid-supercritical state transitions, which are in good agreement with the existing literature of Argon. In conclusion, molecular dynamics simulations can be used to obtain the phase diagram of Argon.

I. INTRODUCTION

Ever since the industrial revolution, there has been a special interest in understanding the thermodynamical properties of gases. Argon has been of particular interest due to its widespread use in both scientific and industrial applications, and also due to its molecular simplicity: it is monoatomic, non-polar and completely spherical. This makes it the perfect candidate for testing different molecular dynamics simulation tools and calibration of experimental setups [1].

Molecular dynamics uses the ergodic hypothesis to determine macroscopic properties of the system, i.e. '*the time averages of an ergodic system correspond to microcanonical ensemble averages*'. Therefore, by simulating the system for a duration $\tilde{t}$, the thermodynamic magnitude X can be calculated using

$$\langle X \rangle = \frac{1}{\tilde{t}} \int_0^{\tilde{t}} dt X(t) \approx \frac{1}{N_t} \sum_{n=1}^{N_t} X\left(t_n \equiv \frac{n\tilde{t}}{N_t}\right). \quad (1)$$

In this report, we consider a system of N classical particles enclosed in a 3D box of length L with periodic boundary conditions, where the particles are subject to pair interactions following the Lenard-Jones potential. The Lenard-Jones potential is given by

$$U(r) = 4\epsilon \left(\left(\frac{\sigma}{r}\right)^{12} - \left(\frac{\sigma}{r}\right)^{6} \right), \quad (2)$$

where $\epsilon/k_B = 119.8$ K and $\sigma = 3.405$ Å are the fitted parameters for Argon [2].

The aim of this report is to study different tools to create the phase diagram for Argon. We analyse two methods to determine the phase transitions points for Argon corresponding to liquid–gas (l–g), solid–liquid (s–l) and solid–supercritical fluid (s–sf). The methods use the pressure P, the specific heat c_V, the pair correlation function $g(r)$, the mean-squared displacement MSD and the diffusion constant D to identify in which pairs of T, P the transition takes place and also the involved phases.

Firstly, in section II, we describe the setup and algorithm used for the molecular simulation as well as the formulas for the thermodynamic variables stated before. In section III, we perform a list of checks to ensure that the simulation works correctly and then discuss the results for the three different phase transitions mentioned above. Finally, in section IV we end with some conclusions.

II. METHODOLOGY

A. MOLECULAR DYNAMICS SIMULATION

The thermodynamical observables are calculated by means of time averages using Eq. (1). Thus, we need to simulate the time evolution of the Argon system. The integration of the Newton's equations of motion is performed using the velocity-Verlet algorithm [2] and using the following units: length in units of σ and energy in units of ϵ (see subsec-

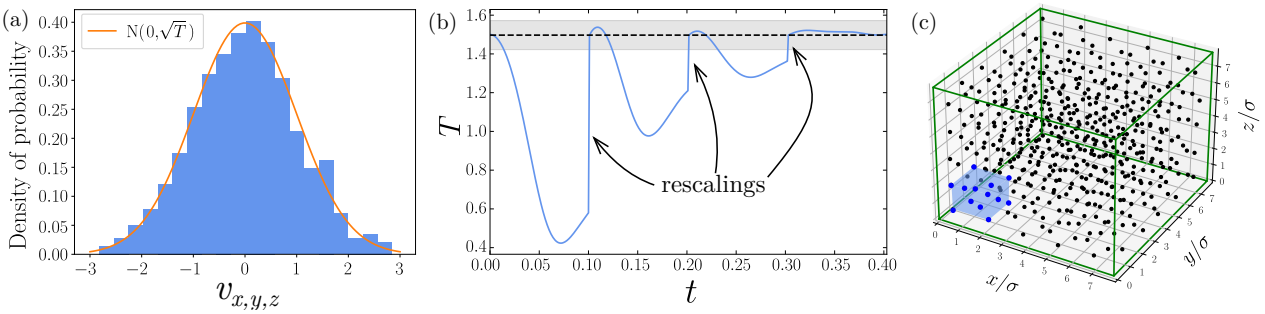

FIGURE 1: Example of (a) the distribution of velocities after thermalization, (b) thermalization or rescaling of the velocities, and (c) initial position of the particles for a system of $N = 500$, $L = 7.857$, and $T = 1.5$ ($\tilde{t} = 0.4$ and $N_t = 1000$). The initial velocities follow the Maxwell-Boltzmann distribution and after thermalization they still keep this distribution, as shown in (a). During thermalization, there is a continuous exchange between potential and kinetic energy (keeping the total energy constant) that prevents the temperature from remaining constant, as depicted in (b). The velocities are rescaled multiple times until the kinetic energy is established according to the desired temperature (shown with a dashed black line, and the tolerance in a grey shade). An FCC cell is highlighted in blue in (c).

tion V-A for more details about the natural units and for the conversion factors used). From now on, all expressions are given in these natural units.

The evolution of positions and velocities of all particles in the system between t and $t + h$ is given by

$$\begin{aligned} \mathbf{x}(t+h) &= \mathbf{x}(t) + h\mathbf{v}(t) + \frac{h^2}{2}\mathbf{F}(\mathbf{x}(t)), \\ \mathbf{v}(t+h) &= \mathbf{v}(t) + \frac{h}{2}\left[\mathbf{F}(\mathbf{x}(t+h)) + \mathbf{F}(\mathbf{x}(t))\right], \end{aligned} \tag{3}$$

where $\mathbf{F} = -\boldsymbol{\nabla} U(\mathbf{x})$, $h = \tilde{t}/N_t$, $\mathbf{x} \equiv \{x_{i,\alpha}\}$ and $\mathbf{v} \equiv \{v_{i,\alpha}\}$ with $i = 1, ..., N$ and $\alpha = x, y, z$ [3]. The periodic boundary conditions are implemented following the minimum image convention [2].

The system is initialized with N particles at the positions of an FCC lattice of length L with random velocities following the Maxwell-Boltzmann distribution for a given temperature [2]; an example of such a distribution is given in Figure 1(a). Therefore, the input parameters of the simulation are N, V, T. Nevertheless, as we work in the microcanonical ensemble (fixed energy by conservation), the temperature is not conserved. We implement a mechanism of velocity rescaling that forces the system to acquire a desired temperature (see Figure 1(b)), which is given by

$$\mathbf{v} \to \lambda \mathbf{v}, \quad \text{with } \lambda = \sqrt{\frac{3(N-1)T}{\sum_{i,\alpha} v_{i,\alpha}^2}}. \tag{4}$$

B. MACROSCOPIC OBSERVABLES

The observables mentioned in section I are determined using Eq. (1) and the expressions listed below. For the observables with time averages, we use the methods of data blocking and autocorrelation function to assess their errors; see subsection V-B for a more detailed description. The errors reported in this work are calculated as the average of the errors from data blocking and autocorrelation function.

- **Specific heat**. From the fluctuations of the kinetic energy E_K and the expression in Lebowitz *et al.* [4],

$$c_V = \left(\frac{2}{3} - N\frac{\langle E_K^2\rangle - \langle E_K\rangle^2}{\langle E_K\rangle^2}\right)^{-1}. \tag{5}$$

- **Pair correlation function**. By making a histogram $n(r)$ of all particle pairs within a distance $[r, r + \Delta r]$, where Δr is the bin size,

$$g(r) = \frac{2V}{N(N-1)}\frac{\langle n(r)\rangle}{4\pi r^2 \Delta r}. \tag{6}$$

  In solids, the pair correlation function has clear peaks located at the relative distance of the atoms inside the crystalline cell [5]. In liquids, we see a peak around σ and for $r > \sigma$ it oscillates around a constant value. In gases, $g(r)$ has the same shape as in liquids but without a (or a much smaller) peak around σ.
- **Mean-squared displacement**. For this magnitude, we use the average over all particles, represented by $\langle\cdot\rangle_{part}$,

$$MSD(t) = \langle|\mathbf{x}(t) - \mathbf{x}(0)|^2\rangle_{part}, \tag{7}$$

  which at long times follows $MSD \propto t^\gamma$. The exponent takes the values $\gamma = 2$ for ideal gases (ballistic), $\gamma = 1$ for liquids (diffusion), and $\gamma = 0$ for solids [6].
- **Diffusion constant**. Defining $\tilde{t}$ as the total simulation time, we can approximate the diffusion constant as

$$D = \lim_{t\to\infty}\frac{1}{6t}MSD(t) \approx \frac{1}{6\tilde{t}}MSD(\tilde{t}). \tag{8}$$

- **Temperature**. From the equipartition theorem [6],

$$T = \frac{2E_K}{3(N-1)}, \tag{9}$$

  where the factor -1 is due to the fact that the total velocity in the system is conserved.
- **Pressure**. From the virial theorem [2],

$$\frac{P}{\rho T} = 1 - \frac{1}{3NT}\left\langle\frac{1}{2}\sum_{ij} r_{ij}\frac{\partial U}{\partial r_{ij}}\right\rangle, \tag{10}$$

  where $\rho = N/V$ is the particle density of the system and r_{ij} are the distances between particles i and j.

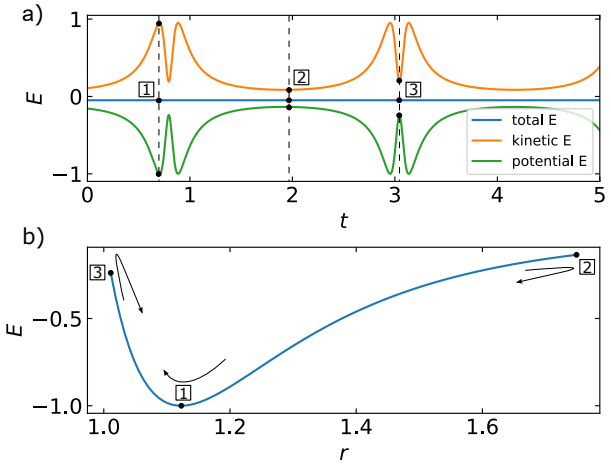

FIGURE 2: (a) Kinetic, potential and total energies for two Argon particles with randomly initialized positions and velocities. (b) Lennard-Jones potential for the range of relative distances in the simulation.

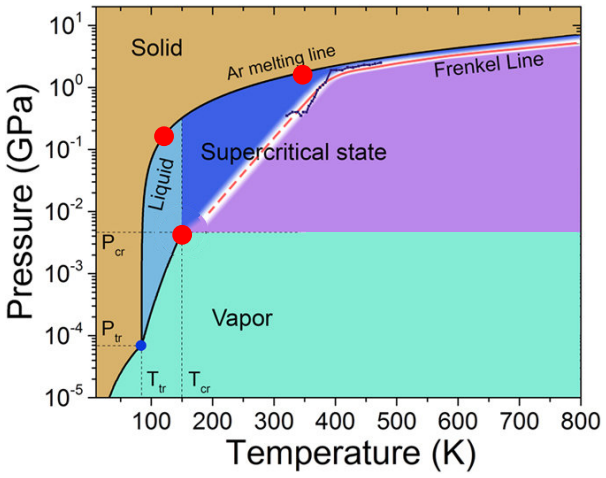

FIGURE 3: Phase diagram of Argon obtained from [8]. The circles in red correspond to the phase transition points studied in this report.

C. METHODS FOR IDENTIFYING PHASE TRANSITIONS

In this report, we analyse two different options for identifying phase transitions: (1) $P(\rho)$ isotherms as done by Verlet [3], and (2) the abrupt change of the observables near the transition point.

The first method is used to identify the critical point. From statistical mechanics, the critical point T_c, P_c fulfills that in the $P(\rho)$ isotherm at T_c there is both an extremal and inflection point located at P_c [7]. Moreover, the $P(\rho)$ isotherms at $T < T_c$ can also be used to calculate the l–g transition points using the Maxwell construction [6].

The second method is used to identify s–l and s–sf transitions. It is based on the abrupt change of the observables when going from solid to any of the other phases [2], in instance

- the diffusion constant for solids is much smaller than for liquids, gases and supercritical fluids,
- the mean-squared displacement at long times is a constant function of time for solids but depends on t^γ for the other phases,
- the specific heat diverges, i.e., $c_V \to \infty$.

III. RESULTS

In this section, we study the performance of the two methods described in section II by selecting three points P_t, T_t corresponding to phase transitions of l–g, s–l, s–sf (see Figure 3) and comparing the obtained numerical results with the literature. Moreover, we also identify the phases involved in the transitions by means of the macroscopic observables and the pair-correlation function to double check that we found the wanted transitions.

Nevertheless, before studying the phase transitions of Argon, we run the checks listed below to ensure that our simulation code works correctly.

- **Energy conservation**. In general, we find that energy is conserved up to a good margin. In simulations with $N = 500$ and 864 particles ($\tilde{t} \in [0.6, 1]$ and $N_t \in [200, 1000]$), we find maximum deviations of the total energy of $E \in (2.5 \cdot 10^{-4}, 3 \cdot 10^{-3})\%$ respectively.
- **Lennard-Jones potential**. In Figure 2(a), we show the typical behaviour of the total, kinetic and potential energies for the case of two Argon particles. In Figure 2(b), we indicate the relative distance and the potential energy between the two particles at the three extremal points of the simulation. The arrows indicate the direction in which the relative position vector is changing at each point. By visual inspection, we can see that the particles behave as expected.
- **Maxwell-Boltzmann distribution**. Figure 1(a) shows that, after the process of thermalization, the particles follow a normal distribution in each of the components, as expected from a system in equilibrium.
- **Specific heat of ideal gas**. For a temperature of $T = 2.49$ and a particle density $\rho = 2.31 \cdot 10^{-3}$, we obtain a specific heat and pressure of $c_V = 1.500 \pm 0.002$ and $P = (5.76 \pm 0.01) \cdot 10^{-3}$, which falls within the margin of the specific heat of an ideal gas. Converting to SI units, these conditions correspond to $T = 298.3$ K and $P = 2.41 \cdot 10^{-4}$ GPa, which are well in the vapor region (see Figure 3).

As we mentioned earlier, temperature is not conserved in the microcanonical ensemble and thus fluctuates. In the following subsections, we will usually not provide the magnitude of these fluctuations due to its computational cost, but we provide here a general estimate. Typical simulations involve $N = 500$ and 864 particles with $\tilde{t} \sim 1$ and $N_t \sim 1000$. Setting the temperature to $T = 1$ and the box length to $L = 7.736$, the relative fluctuations of the temperature are approximately 10% and 8% for $N = 500$ and 864, respectively. In general, the magnitude of the fluctuations decreases as the number of particles simulated increases.

The number of particles N and run times $\tilde{t}$ chosen for the

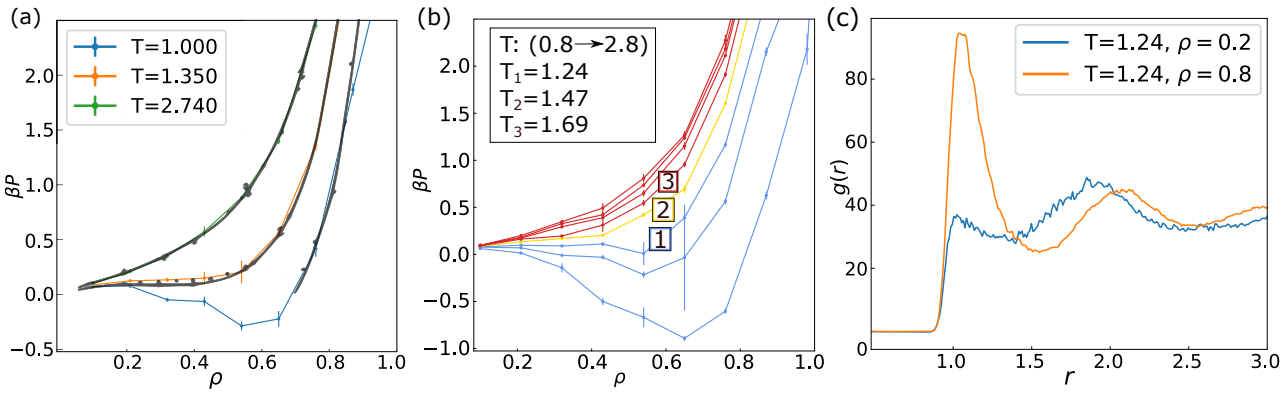

FIGURE 4: (a) Isotherms for three temperatures with superposed data of Figure 2 from [3], (b) isotherms in a range of temperatures covering the critical point, and (c) pair correlation functions for densities $\rho = 0.2$ and $\rho = 0.8$ at temperature $T = 1.24$. These simulations allow us to prove the agreement with previous work with Argon. From (b), we extract a value for the critical temperature of $T_c = 1.4 \pm 0.1$. The pair correlation functions in (c) allow to distinguish, through their shape, the different phases of matter present for low and high densities in each of the isotherms.

simulations will vary. In any case, from multiple simulations, we have observed that setting $\Delta t = \tilde{t}/N_t \in [0.001, 0.003]$ balances accuracy and computational cost. For an overview of the code's efficiency see subsection V-C.

A. LIQUID-GAS TRANSITION AND CRITICAL POINT

Following the work of Verlet in [3], we determine pressure–density isotherms in a range of temperatures corresponding to a l-g transition. By doing so, we get a comparison of the results produced by our code, by Verlet and by experimental data [9]–[11]. Moreover, we establish a possible procedure for studying this transition, recognising the liquid and gaseous phases from the pair correlation function and γ, and finally finding the critical point of Argon.

The simulation setup is the one followed by Verlet: $N = 864$ particles are simulated over a time $\tilde{t} = 0.6$, with a slightly decreased time step, taking $\Delta t = 0.003$ instead of 0.005. Figure 4(a) shows that our results (color lines) mimic those obtained by Verlet (dark lines) and the experimental data (black dots).

In addition, Figure 4(b) shows an extended study of these isotherms. The typical convex-concave form of $P(\rho)$ for T below the critical temperature can be observed for $T < T_1 = 1.24$, which indicates the presence of a critical point. When going from high to low temperature, the first isotherm to manifest an extremal point corresponds to the critical temperature. Therefore, we can recognise the critical temperature to be at $T_c \in (1.24, 1.47)$, between T_1 and T_2. Verlet reports critical temperatures in a range $T_c \in (1.32, 1.36)$, which agree with our results. We can also give a rough estimate of the critical density by visual inspection of Figure 4. We approximate the critical density as the middle point between the two inflexion points of the isotherms T_1 and T_2, giving $\rho_c \in (0.3, 0.5)$ which coincides with $\rho_c \in (0.32, 0.36)$ reported by Verlet. From the graph, giving a value of the critical pressure is not possible within reasonable uncertainty. Nevertheless, through a closer analysis of the isotherms, based on iteratively enclosing the critical point, this method would lead to estimates of these values with uncertainties depending only on the precision of the different observables $(\Delta\rho, \Delta T, \Delta P)$. For $T > T_3 = 202$ K and $\rho > \rho_c$, Argon is found to be in a vapor supercritical state transition, as can be seen in Figure 3.

One would expect that in a realistic simulation we would not be able to see the convex-concave form of the isotherms, which correspond to unstable configurations. In these regions, the actual curve is flattened, representing metastable states, i.e. supercooled vapor and overheated liquid [7]. However, due to the periodic boundary conditions, the coexistence of various phases of matter is impeded [3].

Finally, we show a method to recognise the two phases of matter along the curve of T_1 by means of the pair correlation function and the MSD. Figure 4(c) shows the pair correlation function corresponding to two different points along the curve $T = 1.24$. For the lower density $\rho = 0.2$, we can observe a shape corresponding to that of an interacting gas, while for the higher density $\rho = 0.8$ we recognise the characteristic shape of liquid's pair correlation function [12]. The second indicator of the phase is given by the exponent γ, which is computed by fitting the MSD to $B \cdot t^{\gamma}$. We obtain $\gamma = 1.93 \pm 0.01$ for $\rho = 0.2$ and $\gamma = 1.00 \pm 0.01$ for $\rho = 0.8$, corresponding respectively to gaseous and liquid phases as commented in subsection II-B. These values of γ have been obtained for long enough $\tilde{t}$ so that we avoid the t^2 behaviour for $t \to 0$, but short enough so that not many particles cross the walls of the box. This is needed due to a defect in the computation of the MSD, which does not keep track of the particles once they cross a wall.

B. SOLID-LIQUID TRANSITION

For the solid-liquid transition, we use the second method to find the melting pressure of Argon at $T = 1$, as depicted in Figure 3 ($T = 119.8$ K in SI units). In order to do so, we fix the temperature of the system and scan different box sizes while studying the behaviour of the diffusion constant, the exponent γ and the specific heat. This scan corresponds to

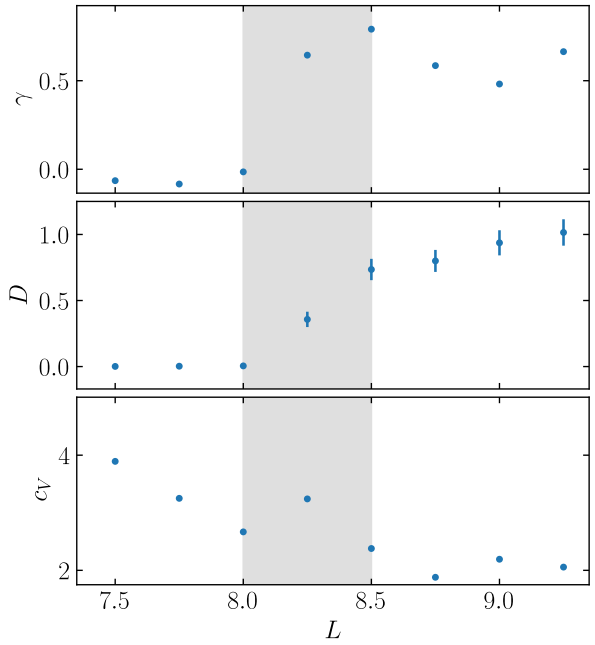

FIGURE 5: Scan of the exponent γ, difussion constant D and specific heat c_V as a function of the box length L at a fixed temperature of $T = 1$. The zone shadowed in gray represents the range of L in which there is an abrupt change of the observables corresponding to the transition between solid and liquid.

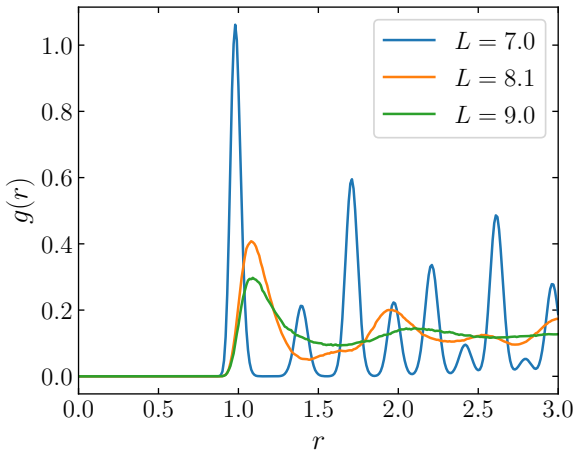

FIGURE 6: Pair correlation function for different box lengths at $T = 1$. Argon behaves as a solid at $L = 7$ and as a liquid at $L = 9$. The transition from solid to liquid is around $L = 8.1$ as the shape of $g(r)$ is in-between solid and liquid. The results have been obtained using $N = 500$, $\tilde{t} = 2$ and $N_t = 2000$.

moving in a vertical line through the $P - T$ phase diagram.

Firstly, we start with a box length corresponding to the solid crystalline form of Argon, which has a lattice constant of $a = 1.5471$ [13], to ensure that we start from a solid state. The phase of the Argon is inquired using the pair correlation function, see Figure 6, which matches with solid state. Then, we increase the box size until $g(r)$ changes from solid to liquid as described in section II. Finally, we do a more refined scan around the transition point found before to improve the accuracy.

The procedure described above has been performed with a system of $N = 500$ particles simulated for $\tilde{t} = 2$ and $N_t = 2000$. The results of the diffusion constant, the exponent γ and the specific heat as a function of the box length in the refined scan are shown in Figure 5. They show an abrupt change of γ and D around $L = 8$ and 8.5, i.e. γ jumps from ~ 0 to ~ 0.5 and D jumps from ~ 0.01 to ~ 0.8. Due to taking a long run time, the exponent γ does not match the expected value of $\gamma_{liquid} = 1$ because we have a higher number of particles crossing the boundaries (as explained previously). For the case of the specific heat, the change is not as clear as in the previous observables, we only see a small increase around $L = 8.25$. However, not observing the divergence of c_V may be due to $\Delta L = 0.25$ and they do not match the specific transition point. For example, computing the c_V at $L = 8.1$ results in $c_V = 5.20 \pm 0.01$, which shows a bigger jump.

From these results and computing the pressure, we can state that the transition s–l takes place at $T \in (0.95, 1.03)$ and $P \in (2.5, 3.3)$, which in SI units correspond to $T \in (114, 124)$ K and $P \in (0.11, 0.15)$ GPa. This range matches the values reported in [8] of $P(T = 120\ \text{K}) = 0.15$ GPa (see Figure 3). Noteworthy, the range of the temperature is determined by the minimum and maximum values that it takes during the simulations of $L = 8.25$ and the range of the pressure corresponds to P at $L = 8$ and $L = 8.5$.

Regarding the robustness of the observables to identify the s–l transition, the exponent γ has the sharpest change around the transition point and therefore it is the best one for finding the transition point. The diffusion constant shows a big jump around the transition point but not as sharp as γ. Finally, as stated before, the increase in the specific heat is small and could not be used alone to identify the phase transition; had we done steps of $\Delta L = 0.5$ it would not have been observed. Nevertheless, it could be used as a check for how close we are to the transition point as the closer we are, the larger c_V diverges.

As a final remark, we have not used the pair correlation function to find the transition point, just to find two points $(L, T = 1)$ such that they are solid and liquid to select the initial and final values for the scan. The reason behind this usage is that the computational cost of determining $g(r)$ is higher than the one of all the other observables together, and that its interpretation is rather qualitative (as it is based on the shape, see Figure 6).

C. SOLID-SUPERCRITICAL STATE TRANSITION

The procedure to find the solid-supercritical state transition point is very similar to the previous section, but in this case we scan over the temperature for a fixed box size. The reason for this choice is to try a different approach than in the solid-liquid transition in order to compare them. Therefore, we use the same simulation conditions as in s–l transition, i.e. $N =$

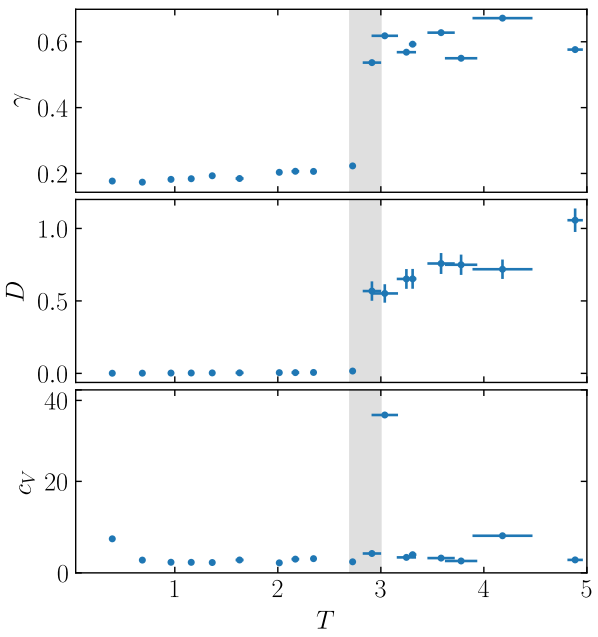

FIGURE 7: Scan of the exponent γ, difussion constant D and specific heat c_V as a function of the temperature at a fixed box size $L = 7.736$. The zone shadowed in gray represents the range of T in which there is an abrupt change of the observables corresponding to the transition between solid and supercritical state.

500, $\tilde{t} = 2$ and $N_t = 2000$.

Again, we start with a box length corresponding to the solid crystalline form of Argon ($a = 1.5471$ and $N = 500$ leads to $L = 7.736$, thus this will be our fixed box size) and a temperature low enough such that we ensure it is a solid (using visual inspection of $g(r)$), i.e. $T = 0.02$. The scan of temperatures with the results of γ, D and c_V is shown in Figure 7. The behaviour of these observables is very similar to Figure 5 for the case of s–l transition. The main differences is that in this case D has a sharper jump and that the c_V shows a clear divergence (although it is a little bit shifted from the jump of D and γ).

From the pressure calculation, we can state that the transition s–sf takes place at $T \in (2.7, 2.9)$ and $P \in (22, 28)$, which in SI units correspond to $T \in (324, 348)$ K and $P \in (1.01, 1.11)$ GPa. This range matches the values reported in [8] of $P(T = 340\ \text{K}) = 1.1$ GPa (see Figure 3). In order to improve the accuracy of the results, we would need to increase the number of particles in the simulation to reduce the fluctuations of T as a function of time. However, we leave this improvement as a future work as our aim in this report is just to prove that this method can be used for finding and identifying transition points.

Comparing the scan over temperature and the one over the box length, we can see that both can be used to identify phase transitions. The advantage of scanning over L is that the temperature is fixed so the scan corresponds to a vertical line in the $P - T$ phase diagram, which is easier to interpret. However, the temperature is not actually constant in all the points and thus there is an extra error to take into account. This fluctuation does not affect that much the scan over the temperature because the box length is correctly fixed, but then the points in T are not equally spaced.

As a final remark about robustness, in this case both γ and D show a sharp jump around the transition point compared to the s–l transition. Moreover, we can also see a clear divergence of c_V when close to the transition, although it is a little bit off from the abrupt change of γ and D as specified before.

IV. CONCLUSIONS

The described methods in this report constitute a set of tools sufficient to produce a phase diagram of any substance well described by Lenard-Jones pairwise interaction. In order to validate the method, we have chosen Argon as a study case and compared the obtained results with those of the literature.

By analyzing pressure-density isotherms we are able to locate the critical point at $T_c \in (1.24, 1.47)$ and $\rho_c \in (0.3, 0.4)$, in agreement with the experimental data. Then, making use of the behaviour of different observables at the phase transitions, we are able to find the transition points in solid-liquid at $T \in (0.95, 1.03)$, $P \in (2.5, 3.3)$ and liquid-supercritical state transitions at $T \in (2.7, 2.9)$, $P \in (22, 28)$, in agreement with [8]. In a similar manner, from the specific values of those observables and the shape of the pair correlation function, we are able to successfully discern the phase of matter at any given point.

The accuracy of the methods here described rely on the algorithm chosen for the time evolution, and the choices of N, N_t and $\tilde{t}$, which implies that the computational cost is of great relevance. Our simulations are based on the Verlet algorithm, which is a second order symplectic integrator. However, higher order integrators exist and could be implemented in order to increase the accuracy [14]. In addition, this may be combined with Barnes-Hut's approximation algorithm [15], which decreases the computational effort from the current brute force approach $O(N^2)$ to $O(N \log N)$. These two changes would allow to increase the number of particles and the run time (keeping Δt the same), leading to better averages over time and particles, without a mayor increase in the computation time.

The importance of increasing the time efficiency becomes evident if we explicitly look at the computation time to generate the data of Figure 4, which takes ~ 2 h (~ 2 min per data point). With the analysis performed in subsection V-C we know the main contribution is the time evolution of the particle ensemble (in particular the computation of the force), thus the changes proposed in the previous paragraph would have significant impact.

On a different note, our approach of symplectic integrators leads to an implementation of the microcanonical ensemble. However, this is not ideal, for example, for analysing isotherms, because of the temperature fluctuations. As future work, it could be then investigated whether implementing a canonical ensemble as described in [16] is beneficial.

REFERENCES

[1] C. Tegeler, R. Span, and W. Wagner, "A new equation of state for argon covering the fluid region for temperatures from the melting line to 700 k at pressures up to 1000 mpa," Journal of Physical and Chemical Reference Data, vol. 28, no. 3, pp. 779–850, 1999. [Online]. Available: https://doi.org/10.1063/1.556037

[2] J. Thijssen, Computational Physics, 2nd ed. Cambridge University Press, 2007.

[3] L. Verlet, "Computer 'experiments' on classical fluids. i. thermodynamical properties of lennard-jones molecules," Phys. Rev., vol. 159, pp. 98–103, Jul 1967. [Online]. Available: https://link.aps.org/doi/10.1103/PhysRev.159.98

[4] J. Lebowitz, J. Percus, and L. Verlet, "Ensemble dependence of fluctuations with application to machine computations," Physical Review, vol. 153, no. 1, p. 250, 1967.

[5] T. Group, "The radial distribution function for liquids, solids and gases."

[6] L. E. Reichl, "A modern course in statistical physics," 1999.

[7] D. Voskresensky, "Evolution of quasiperiodic structures in non-ideal hydrodynamic description of phase transitions," 01 2020.

[8] D. Bolmatov, M. Zhernenkov, D. Zav'yalov, S. N. Tkachev, A. Cunsolo, and Y. Q. Cai, "The frenkel line: a direct experimental evidence for the new thermodynamic boundary," Scientific reports, vol. 5, no. 1, pp. 1–10, 2015.

[9] J. Levelt, "The reduced equation of state, internal energy and entropy of ar and xe," Physica, vol. 26, no. 361-377, 1960.

[10] W. V. Witzenburg, "Unpublished," Dissertation Abstracts, vol. 25, no. 1268, 1964.

[11] A. V. Itterbeck, . Verbeke, and K. Staes, Physica, vol. 29, no. 742, 1963.

[12] D. Bolmatov, D. Zav'yalov, M. Zhernenkov, E. Musaev, and Y. Cai, "Unified phonon-based approach to the thermodynamics of solid, liquid and gas states," Annals of Physics, 09 2015.

[13] C. Barrett and L. Meyer, "X-ray diffraction study of solid argon," The Journal of Chemical Physics, vol. 41, no. 4, pp. 1078–1081, 1964.

[14] E. Forest and R. D. Ruth, "Fourth-order symplectic integration," Physica D: Nonlinear Phenomena, vol. 43, no. 1, pp. 105–117, 1990.

[15] J. Barnes and P. Hut, "A hierarchical o(n log n) force-calculation algorithm," Nature, vol. 324, p. 446–449, 1986.

[16] S. Nosé, "A molecular dynamics method for simulations in the canonical ensemble," Molecular Physics, vol. 52, no. 2, pp. 255–268, 1984.

[17] J. R. de Laeter, J. K. Böhlke, P. D. Bièvre, H. Hidaka, H. S. Peiser, K. J. R. Rosman, and P. D. P. Taylor, "Atomic weights of the elements. review 2000 (iupac technical report)," Pure and Applied Chemistry, vol. 75, no. 6, pp. 683–800, 2003.

V. SUPPLEMENTARY INFORMATION

A. NATURAL UNITS

To avoid round-off errors in the numerical results, we have adopted a dimensionless system of units that is natural to the molecular dynamics simulation of Argon.

We first set the units of position and energy as the effective diameter of an atom of Argon, σ, and the depth of the Lennard-Jones potential well, ϵ, respectively. The units of time follow from making the mass m disappear from Newton's equations of motion. Finally, the units of each observable follow simply from turning them dimensionless. In Table 1 we summarize these transformations.

TABLE 1: Transformation from natural to SI units. The variables in natural units are denoted as x' and in SI units as x. Note that the mass of an atom of Argon is $m = 6.63 \cdot 10^{-26}$ kg [17].

Transformation	Numerical value
$r = r'\sigma$,	$\sigma = 3.405$ Å
$E = E'\epsilon$	$\epsilon = 1.65 \cdot 10^{-21}$ J
$t = t'\sigma\sqrt{m/\epsilon}$	$\sigma\sqrt{m/\epsilon} = 2.156 \cdot 10^{-12}$ s
$T = T'\epsilon/k_B$	$\epsilon/k_B = 119.8$ K
$P = P'\epsilon/\sigma^3$	$\epsilon/\sigma^3 = 41.9$ MPa
$D = D'\sigma\sqrt{\epsilon/m}$	$\sigma\sqrt{\epsilon/m} = 5.38 \cdot 10^{-8}$ m^2/s
$c_V = c_V' k_B$	$k_B = 1.38 \cdot 10^{-23}$ J/K

B. ERROR ESTIMATION FOR OBSERVABLES

The data from the simulation is correlated because during the time evolution the next state is a small variation of the previous one. Therefore, the error for the results cannot be calculated by the usual standard deviation formula because it assumes independent data. In order to estimate such error, we use two different approaches: (1) autocorrelation function and (2) data blocking [2].

The autocorrelation function for the observable $A(t)$ is defined as

$$\chi_A(m) = \frac{(N_t - m)\sum_n A_n A_{n+m} - (\sum_n A_n)(\sum_n A_{n+m})}{(N_t - m)\sqrt{F(0)\cdot F(m)}} \tag{11}$$

where $F(m) = \sum_n A_{n+m}^2 - (\sum_n A_{n+m})^2$, $\sum_n \equiv \sum_{n=1}^{N_t - m}$ and $A_n \equiv A(t_n)$. By fitting $\chi_A(m)$ to $e^{-m/\tau}$, one can extract the correlation time τ, which is used to estimate the error of A using

$$\sigma_A = \sqrt{\frac{2\tau}{N_t}\left(\langle A^2\rangle - \langle A\rangle^2\right)}. \tag{12}$$

For the data blocking, the data $\{A_n\}_{n=1}^{N_t}$ is split in N_b blocks of size b (with $N_b = N_t/b$). Taking the average of A in each of the blocks results in a new array of values $\{a_i\}_{i=1}^{N_b}$. Then, we compute the standard deviation of a, given by

$$\sigma_a(b) = \sqrt{\frac{\langle a^2\rangle - \langle a\rangle^2}{N_b - 1}}. \tag{13}$$

Finally, the error of A (i.e. σ_A) is given by the value of σ_a when $\sigma_a(b)$ has converged to a roughly constant value.

In this report, we have calculated σ_A by means of the two methods, which both show similar values. As it is not trivial how to choose the limits for fitting $e^{-m/\tau}$ in the autocorrelation function or to determine when $\sigma_a(b)$ is constant in the data blocking, we have tried different options and tested them with synthetic correlated data. In particular the best methods we found are

- **Autocorrelation function**. Get $\tilde{\tau}$ such that $\chi_A(\tilde{\tau}) = 1/e$, and then do the fitting in $m \in [0, 3\tilde{\tau}]$ to get τ.
- **Data blocking**. Get $\tilde{b}$ such that $\sigma_a(\tilde{b}) > \sigma_a(\tilde{b}+1)$, and then fit $\sigma_a(b)$ to $B - Ce^{-A\cdot b}$ from $b = 2$ to $b = 4\tilde{b}$ in order to get $\sigma_A = B$.

C. CODE EFFICIENCY

Molecular dynamics simulations can become CPU intensive very easily if care is not taken while writing the code. For that reason, we analysed the code performance using a line profiler. For the analysis, we produce two experiments: Computing the specific heat for a range of 6 temperatures, and produce pair correlation functions in two different setups: solid and gaseous phases. The results are reported in the Table 2.

TABLE 2: Relative run times between executed functions when computing (1) $c_v(T)$ for 6 temperatures and (2) pair correlation function for 2 temperatures. The simulation setup is: $N = 500$, $\tilde{t} = 0.8$, $N_t = 500$. The simulations took 350 s and 365 s respectively.

$c_v(T)$		$g(r)$	
Executed function	Run time (%)	Executed function	Run time (%)
simulate	66.1	simulate	20.2
get_equilibrium	30.7	get_equilibrium	19.7
specific_heat	3.1	pair_correlation	60.0
rest	0.1	rest	0.1

In the light of these results, we can conclude several things. For observables such as the specific heat, pressure, or the diffusion coefficient, most of the computational effort depends on the simulation functions, that is, performing the time evolution of the system. Whereas, for the pair correlation function this is not the case. This function requires many computations, which explains that it required higher percentage than the time evolution.

A small attempt to further optimize the time evolution was made, which consisted in truncating the force computation to a distance of 3σ. However, the results in terms of efficiency remained similar. On the other hand, the pair correlation function is computed a very limited amount of times, so it does not require any optimization.